ADVANCED FUNCTIONAL MATERIALS

DOI: 10.1002/adfm.200600935

1D and 3D Ionic Liquid–Aluminum Hydroxide Hybrids Prepared via an Ionothermal Process**

By *HoSeok Park*, *Yeong Suk Choi*, *YoJin Kim*, *Won Hi Hong*,* and *Hyunjoon Song*

Room-temperature ionic liquids (RTILs) are used as hierarchically multifunctional components by employing them not only as templates and co-solvents for fabricating nanostructured materials but also proton conductors for electrochemical devices. RTIL/aluminum hydroxide (RTIL–Al) hybrids containing various nanometer-sized shapes, including 1D nanorods with hexagonal tips, straight and curved nanofibers, nanofibers embedded in a porous network, and 3D octahedral-, polyhedral-, and angular spherical shapes are synthesized via a one-pot ionothermal process. The structures or shapes of the RTIL–Al hybrids are related to the anionic moieties, alkyl chain length of the RTILs, and the humidity during fabrication. In particular, the introduction of water molecules into the interface led to 3D isotropic growth of the hybrids by influencing intermolecular interactions between the RTILs and the building blocks. The shapes of the nanohybrids fabricated from RTILs containing short alkyl chains were dependent on the types of anions and on the level of humidity. These results indicate that the cooperative interactions between RTILs and aluminum hydroxides induces emerging shape-controlled hybrids. The shape-controlled nanohybrids show enhanced electrochemical properties compared to those of a conventional hybrid prepared by mixing RTILs and aluminum hydroxides, exhibiting tenfold or higher proton conductivity under anhydrous condition and thermal stability as a result of the continuous proton conduction channel and the one-pot-assembled nanoconfinement. This method is expected to be a useful technique for controlling the diverse shapes of nanometer-sized crystalline inorganic materials for a variety of applications, such as fuel cells, solar cells, rechargeable batteries, and biosensors.

1. Introduction

Thus far, a lot of effort has been concentrated on controlling the shapes and structures of nanometer-sized functional materials because of their unique properties in electronic or ionic transportation for applications in electrochemical and optical devices.[1] For the purpose of fabricating nanostructured materials, room-temperature ionic liquids (RTILs) have received a lot of attention as templates or co-solvent systems in recent years.[2–4] Ionothermal synthesis, which relies on the ionic characteristic of RTILs, has advantages over conventional solution syntheses in terms of eliminating the complications associated with high hydrothermal pressures in a sealed autoclave and avoiding the post-addition of organic solvents.[5,6] Diverse cooperative interactions between inorganic species and templates drive a variety of complex nanostructures and nanometer-sized shapes from inorganic or hybrid materials via organization and transformation.[7,8] In addition, sensitive modulation of the physical/chemical environment at the interfaces between building units and templates induces higher-order architectures via supramolecular complementarities.[7,8] In RTIL-templated systems, the appropriate combination of anions or interactive components with cations of RTILs may enhance the diversity of cooperative interactions between RTILs and the building blocks. Thus, it is hypothesized that the changes in the chemical environment as a result of the introduction of an interactive component such as water into the interface can trigger the emergence of various shapes by influencing the force fields of secondary interactions, that is, hydrogen bonding or van der Waals forces.

From an applications point of view, pristine RTILs confront few limits to electrochemical devices because of their fluidic properties and low viscosity. Therefore, RTILs are usually incorporated into or hybridized with solid matrices such as polymers or inorganic materials.[9,10a] However, the ionic conductivities of composite materials are much lower than those of pristine RTILs as a result of the inefficient proton-conducting channels and interfacial resistance between RTILs and the solid matrixes. In order to overcome these problems, a one-pot assembled nanoconfinement of RTILs inside an integrated sys-

[*] Prof. W. H. Hong, H. S. Park, Dr. Y. J. Kim
Department of Chemical and Biomolecular Engineering
Korea Advanced Institute of Science and Technology (KAIST)
Guseong-dong 373-1, Yusong-gu, Daejeon (Republic of Korea)
E-mail: whhong@kaist.ac.kr
Dr. Y. S. Choi
Energy & Materials Research Lab
Samsung Advanced Institute of Technology (SAIT)
P.O. Box 111, Suwon (Republic of Korea)
Prof. Dr. H. Song
Department of Chemistry and School of Molecular Science
Korea Advanced Institute of Science and Technology (KAIST)
Guseong-dong 373-1, Yusong-gu, Daejeon (Republic of Korea)

[**] This work was supported by Brain Korea 21 (BK21) program and New and Renewable Energy Project (Ministry of Commerce, Industry, and Energy). We thank the Korea Basic Science Institute (KBSI) for use of equipment for TEM, SEM, and NMR. Supporting information is available online from Wiley InterScience or from the author.

tem of shape-controlled crystalline hybrid gels for proton conduction are being intensively investigated.[11,12]

Herein, we report a general and facile synthetic method to fabricate various nanometer-sized shapes of RTIL–Al hybrids by controlling the cooperative interaction during an ionothermal process depending on the type of the RTIL and the humidifying conditions, as illustrated in Scheme 1. In this paper, RTILs (multifunctional materials in terms of template agents and co-solvents) are also studied as proton conductors because they act as proton transporting media with substantial self-dissociation abilities owing to their Brönsted acid–base properties.[10]

2. Results and Discussion

Figure 1 presents the shape dependence of RTIL–Al hybrids on the humidifying conditions during the ionothermal treatment using 1-butyl-3-methylimidazolium tetrafluoroborate as a representative RTIL (detailed ionothermal procedures are described in the Experimental section below). Under humidifying conditions, 1-butyl-3-methylimidazolium-tetrafluoroborate/aluminum hydroxide (Hum-C_4BF_4–Al) hybrid exhibited a 3D octahedral shape with a size of ca. 150–250 nm. The selected-area electron diffraction (SAED) pattern of the Hum-C_4BF_4–Al hybrid revealed its crystalline structure with hexagonal symmetry. In contrast, randomly de-bundled 1D nanorods were produced under nonhumidifying conditions (Non-C_4BF_4–Al hybrid), displaying a minimum diameter of ca. 25–50 nm, a maximum diameter of ca. 40–90 nm, and a length of ca. 1.3–1.6 μm. A scanning electron microscopy (SEM) image of the Non-C_4BF_4–Al hybrid after isolation exhibits a 1D nanorod with a hexagonal tip. X-ray diffraction (XRD) data show that both the 1D hexagonal rod-shaped hybrids and the 3D octahedral hybrids were indexed to the hexagonal crystalline phase of aluminum hydroxide,[13] whereas the peak marked with an asterisk at $2\theta = 19.98°$ was ascribed to the stacking of imidazolium rings. The difference in the relative intensities of the XRD peaks corresponding to specific shapes of two C_4BF_4–Al hybrids indicate that the distinct shapes were associated with the optimal directional growth of the aluminum hydroxide crystallites.

In order to determine the effect of the RTILs and humidity on the formation of hybrid nanoparticles, the anionic moieties and alkyl chain length were varied as follows: 1-butyl-3-methylimidazolium bis(trifluoromethylsulfonyl)imide (C_4TFSI), 1-butyl-3-methylimidazolium chloride (C_4Cl), 1-dodecyl-3-methylimidazolium chloride (C_{12}Cl), and 1-hexadecyl-3-methylimidazolium chloride (C_{16}Cl). For the C_4TFSI–Al hybrids, 3D angular spheres were fabricated under the humidifying condition, while 1D straight and long nanofibers were produced under nonhumidifying conditions (Fig. 2a and b, respectively). For the C_4Cl–Al hybrids, a 3D polyhedral shape was created under the humidifying condition, whereas 1D curved and short nanofibers were formed under nonhumidifying conditions (Fig. 2c and d, respectively). Table 1 summarizes the chemical compositions, shapes, and structures of the hybrids according to the types of anions, the alkyl chain length, and humidifying conditions. In this research, we focused on the changes in the anionic moieties, alkyl chain length, and humidity; the effect of the concentration of the RTILs will be reported soon. Quantitative compositions of the respective hybrids revealed the amount of RTILs within a hybrid system. For the formation of the hybrids with a chlorine anion and longer alkyl chains (C_{12} and C_{16}), the C_{12}Cl–Al and C_{16}Cl–Al hybrids displayed the nanostructure consisting of nanofibers embedded in a porous system irrespective of the humidifying condition, similar to the morphology reported by previous references,[14,15] due to increased hydrophobicity (see Supporting Information, Figs. S1 and S2). These findings clarify that the shapes of the nanohybrids fabricated by RTILs that contain short alkyl chains were dependent on the types of anions and on the level of humidity.

The molecular structures of inorganic materials forming specific crystal phases are kinetically tuned by various synthetic conditions such as temperature, pH, stoichiometry, the types of precursors, additives for rate control, templates, etc.[16] Furthermore, the types of RTILs affected the nucleation rate of the aluminum precursors used for the formation of nuclei because of the low interface energy

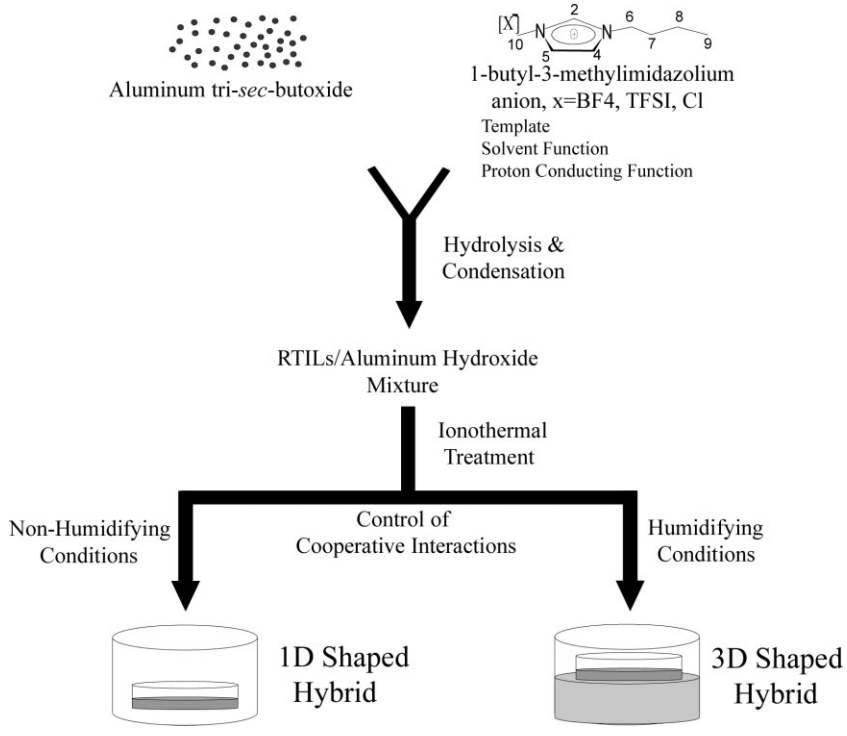

Scheme 1. An illustration for the synthetic process for RTIL–Al hybrids prepared by the dual-functions of 1-butyl-, dodecyl-, or hexadecyl-3-methylimidazolium anion (X = BF_4, TFSI, and Cl) and atom numbering for C_4BF_4.

ADVANCED FUNCTIONAL MATERIALS

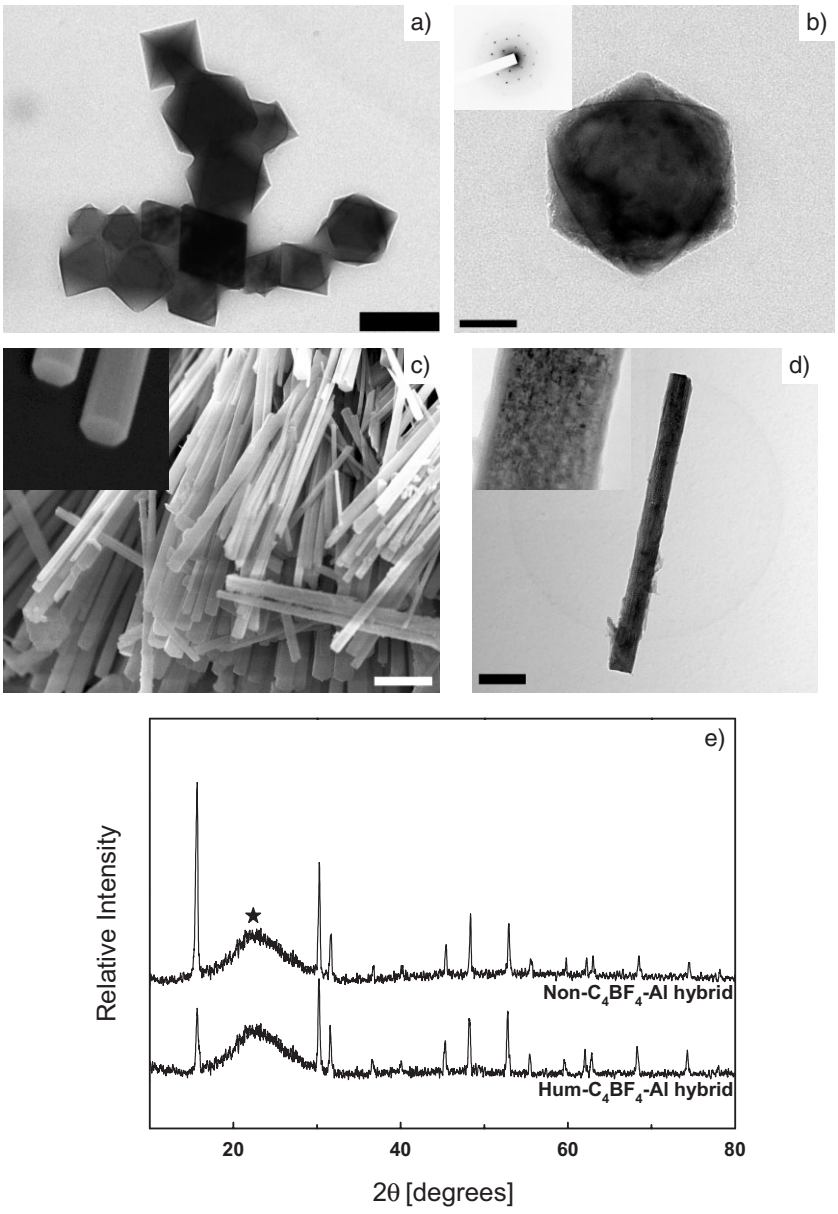

Figure 1. a,b) TEM images (scale bar: 200 nm and 50 nm, respectively) of Hum-C_4BF_4–Al hybrid (inset is the inverse image of the selected-area electron diffraction (SAED) pattern). c) SEM image (scale bar: 200 nm) and d) TEM images (scale bar: 200 nm) of Non-C_4BF_4–Al hybrid. e) XRD patterns of Hum-C_4BF_4–Al and Non-C_4BF_4–Al hybrids.

and high directional polarizability of RTILs in the reaction medium,[17] resulting in different crystal phases. In the case of RTILs used in this research, the polarity and hydrophilicity increase in this order TFSI < BF_4 < Cl and C_{16} < C_{12} < C_4.[18] RTILs with Cl and TFSI anions formed orthorhombic boehmite phases of aluminum hydroxides, while RTILs with BF_4 anions triggered hexagonal crystal phases of aluminum hydroxides. However, alkyl chain length did not change the crystal phases of aluminum hydroxides. Considering that only C_4BF_4, with intermediate hydrophilicity and size among anions and short alkyl chain, induced hexagonal crystal phases of aluminum hydroxides irrespective of humidifying condition, a careful selection of RTILs is required to obtain the desired crystal phase.

The structure formation of the hybrids is explained using Fourier-transform IR (FT-IR), NMR, thermogravimetric analysis (TGA), and N_2 sorption/desorption data. Two peaks above 3000 cm^{-1} in the IR spectra of C_4BF_4–Al hybrids were regarded as diagnostic of the changes in the CH···F hydrogen bonding between the BF_4^- anion and the 4,5-hydrogens of the imidazolium ring, as shown in Figure 3.[19] In RTIL-templated systems, intermolecular interaction, originating from the hydrogen bonding-co-π–π stacking,[4] significantly affected other peaks ascribed to imidazolium rings and anions of C_4BF_4–Al hybrids as well as two peaks above 3000 cm^{-1} (see Supporting Information). The chemical shifts of the imidazolium ring protons in the ^{1}H NMR spectra were also strongly influenced by their chemical surroundings, which could perturb hydrogen bonding (see Table S1). With the different locations of chemical shifts associated with the distinct intermolecular interactions between C_4BF_4 and the aluminum hydroxide crystallites, the chemical shifts of H(5), H(7), H(8), and H(9) moved upfield, while those of the others moved to downfield. In addition, two peaks at 6.5 and 6.3 ppm were assigned to protons of the structured water of Al–OH moieties in aluminum hydroxides. The ^{1}H NMR data suggest that, when water molecules replace the C_4BF_4 anions interacting with neighboring aluminum hydroxide crystallites under the humidifying condition, the force field of hydrogen bonding was perturbed at the interface.

As can be seen in Figure 4, the C_4BF_4–Al hybrids isolated by extraction showed a Type IV hysteresis loops, demonstrating that the RTIL (C_4BF_4) was confined within the mesoporous system of hybrid as a consequence of the formation of cylindrical micelles during hydrolysis and condensation. Two kinds of C_4BF_4–Al hybrids before extraction obtained negligible surface area, that is, below 0.02 $m^2 g^{-1}$, as a result of pore blockage by means of the confinement of C_4BF_4. The complete removal of RTILs (C_4BF_4, C_4TFSI, and C_4Cl) from hybrids by extraction is indicative of open mesoporosity (the absence of C_4BF_4, C_4TFSI, and C_4Cl was verified by elemental analysis). The characteristic XRD peaks of C_4BF_4 (and C_4TFSI, C_4Cl) in the isolated C_4BF_4–Al (and C_4TFSI–Al, C_4Cl–Al) hybrids disappeared, simultaneously conserving hexagonal crystal phases (orthorhombic boehmite) and morphologies of 1D and 3D shaped nanohybrids (see Fig. S3, S4, and S5). When RTILs were removed by calcination at 550 °C, the calcined RTIL–Al

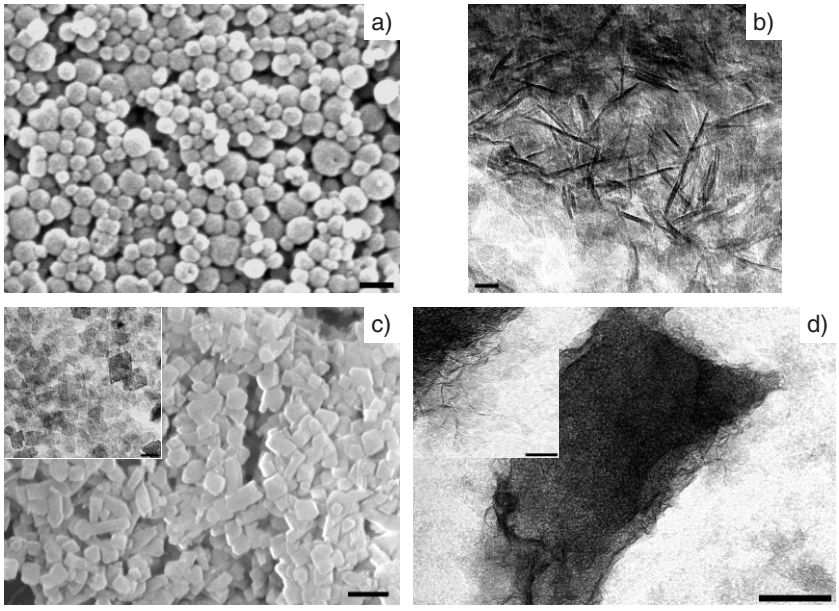

Figure 2. a) SEM image (scale bar: 200 nm) of Hum-C_4TFSI–Al hybrid and b) TEM image (scale bar: 200 nm) of Non-C_4TFSI–Al hybrid. c) SEM image (scale bar: 200 nm) of Hum-C_4Cl–Al hybrid (inset is TEM image (scale bar: 100 nm)) and d) TEM image (scale bar: 200 nm) of Non-C_4Cl–Al hybrid (inset is TEM image (scale bar: 50 nm)).

hybrids exhibited almost the same textural properties and typical Type IV hysteresis loops as the RTIL–Al hybrids isolated by extraction. Thus, FT-IR, ^{1}H NMR, and N_2 sorption/desorption data confirmed that RTILs, which were confined within the cylindrical mesopores of hybrids, interacted with the building blocks consisting of aluminum hydroxide crystallites.

Hum-C_4BF_4–Al hybrid (10.6 wt %) had more structured water compared to that of the Non-C_4BF_4–Al hybrid (9.2 wt %) above 100 °C (see Fig. S6 and the broad peak of the O–H bond at 3200 cm^{-1} of the IR spectra). Sufficient water was adsorbed physically or chemically at the surfaces of the building blocks through intercalation into the interface between C_4BF_4 and aluminum hydroxides under the humidifying condition. Both TGA and FT-IR data suggest that the crucial interface that determines the shape of the hybrids is between the hydroxyl groups of the aluminum hydroxide crystallites and the anions of C_4BF_4 adsorbed at the surface of the building blocks. Furthermore, water molecules altered the cooperative interactions at the crucial interfaces, as the interactive components capped on the building blocks were replaced mainly by water molecules. As an ionothermal treatment was carried out, the characteristic peaks of the BF_4^- anions and imidazolium rings were gradually changed in the process of the relocation and organization of building blocks by means of the interplay between C_4BF_4 and the aluminum hydroxide crystallites, as shown in Figure 5a and b. Both the Hum-C_4BF_4–Al and the Non-C_4BF_4–Al hybrids revealed time-dependent changes in the characteristic peaks of the BF_4^- anions and imidazolium rings, especially around 3000 cm^{-1}, 1460 cm^{-1}, and 1030 cm^{-1}. Despite the identical crystal structure of the two hybrids, the respective changes in the IR spectra of the two hybrids imply that different processes were involved in separate morphological evolutions, resulting in the construction of 1D and 3D shapes. The hydrolytic transformation of hydroxyl (Al–OH) centers to oxo (Al–O–Al) bridges, as shown in the time-dependent weakening of the O–H bond at 3200 cm^{-1}, reduces the surface charge of the building blocks by squeezing out water molecules, thereby inducing their aggregation and organization.[7,14,20] Thus, perturbation of a secondary force field by water intercalation could drive the formation of 3D nanoshapes of hybrids by influencing the hydrolytic transformation process.

Scheme 2 illustrates the proposed mechanism of shape formation of RTIL–Al hybrids. Aluminum hydroxide crystallites consisting of nuclei of respective crystal phases form building blocks via nucleation and growth steps during an ionothermal process. The surfactant-induced fiber formation (SIFF) mecha-

Table 1. Chemical composition, shape, and structure of RTIL–Al hybrids dependant on the anion moieties, alkyl chain length, and humidifying condition.

Alkyl chain	Type of anion	Humidifying conditions	Quantitative analysis (wt % of RTILs) [a]	Shape	Structure [b]	Notation
C_4	BF_4	No	51.82	1D nanorod with hexagonal tip	Hexagonal	C_4BF_4
C_4	BF_4	Yes	49.52	3D octahedral shape	Hexagonal	C_4BF_4
C_4	TFSI	No	69.99	1D straight and long nanofiber	Orthorhombic (Boehmite)	C_4TFSI
C_4	TFSI	Yes	69.42	3D angular sphere	Orthorhombic (Boehmite)	C_4TFSI
C_4	Cl	No	47.59	1D curved and short nanofiber	Orthorhombic (Boehmite)	C_4Cl
C_4	Cl	Yes	46.66	3D polyhedral shape	Orthorhombic (Boehmite)	C_4Cl
C_{12}	Cl	No	54.83	1D nanofibers embedded in a porous network	Orthorhombic (Boehmite)	C_{12}Cl
C_{12}	Cl	Yes	55.38	1D nanofibers embedded in a porous network	Orthorhombic (Boehmite)	C_{12}Cl
C_{16}	Cl	No	65.99	1D nanofibers embedded in a porous network	Orthorhombic (Boehmite)	C_{16}Cl
C_{16}	Cl	Yes	64.08	1D nanofibers embedded in a porous network	Orthorhombic (Boehmite)	C_{16}Cl

[a] Chemical compositions of RTILs within respective hybrids were evaluated by elemental analysis. [b] Crystalline structures of aluminum hydroxides induced by the respective RTIL and experimental conditions were evaluated by XRD data.

ADVANCED FUNCTIONAL MATERIALS

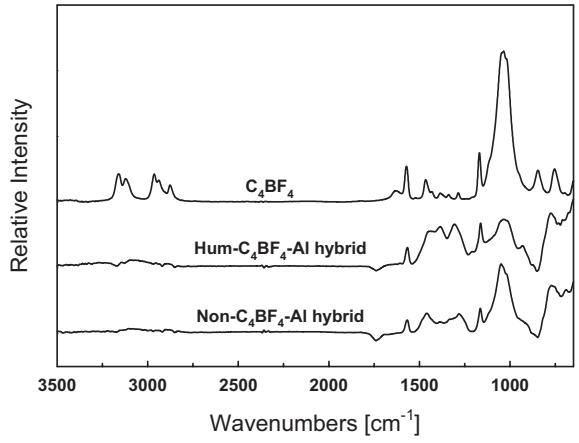

Figure 3. FT-IR spectra of C_4BF_4, Hum-C_4BF_4–Al hybrid, and Non-C_4BF_4–Al hybrid.

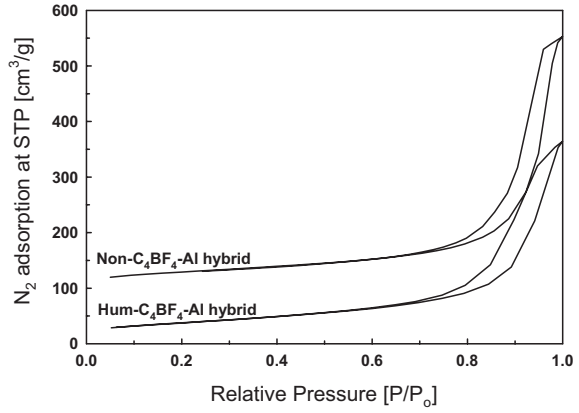

Figure 4. Nitrogen adsorption/desorption isotherms of Hum-C_4BF_4–Al and Non-C_4BF_4–Al hybrids after removing C_4BF_4 by extraction.

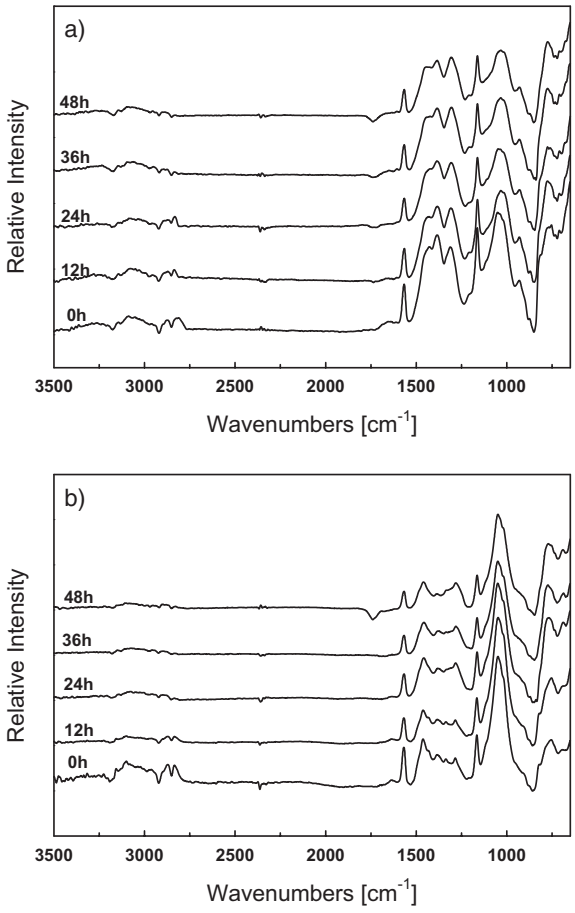

Figure 5. FT-IR spectra of a) Hum-C_4BF_4–Al and b) Non-C_4BF_4–Al hybrids as a function of reaction time during an ionothermal process.

nism based on biomineralization, as proposed by Zhu et al. explains that 1D nanoshape of boehmite was induced by intermolecular interaction via hydrogen bonding between templates and building blocks.[7,14] Similar to the SIFF mechanism,[14] shapes and structures of hybrids in this ionothermal process were triggered by intermolecular interaction between anions of RTILs (constituting cylindrical micelles) and aluminum hydroxide crystallites (constituting building blocks). Several researchers have demonstrated that molecules, ligands, or functional groups adsorbed on building blocks drive the emergence of superstructures of materials via aggregation and organization.[7,8,21] Therefore, cooperative interactions via hydrogen bonding and π–π stacking induced the realignment of building blocks along a specific direction with the minimization of surface energy, followed by transformation into specific shapes of RTIL–Al hybrids. Considering that the diverse morphologies of identical mineral crystallites were attributed to the differences in the surface energy of respective crystal faces and in external growth circumstance,[22] the 3D shape of the hybrid was obtained by growing more isotropically, as a consequence of altering the surface energy of the crystal face or the local environment at the interface through water intercalation. Therefore, as a result of the appropriate combination of RTILs with a short alkyl chain (C_4) and humidity, the changes in the cooperative interactions generated the distinct shapes and molecular organization of hybrids because the type of anion of the RTIL determines the polarity and hydrophilicity, while the introduction of water molecules perturbs the interplay of RTILs and building blocks via hydrogen bonding.

For application as anhydrous proton-conducting materials for fuel cells, reasonable proton conductivities and thermal stabilities above 100 °C are required. Thermal stabilities of the nanohybrids were based on the decomposition of C_4BF_4 confined within the mesopores of hybrid system above 400 °C, as shown in TGA data. In addition, the C_4BF_4–Al hybrids were cast on glasses as a thin film (Fig. 6a). The Non-C_4BF_4–Al hybrid was more transparent than the Hum-C_4BF_4–Al hybrid, indicative of the differences in the miscibility. However, the C_4BF_4/AlOOH mixture prepared by physical mixing of C_4BF_4 and aluminum hydroxide could not be cast as a film. The proton conductivities of two C_4BF_4–Al hybrids were compared to those of C_4BF_4/AlOOH (60 wt % of C_4BF_4), as shown in Figure 6. In the hybrid system, a typical complex impedance plot exhibited a feature similar to that of a highly proton conduct-

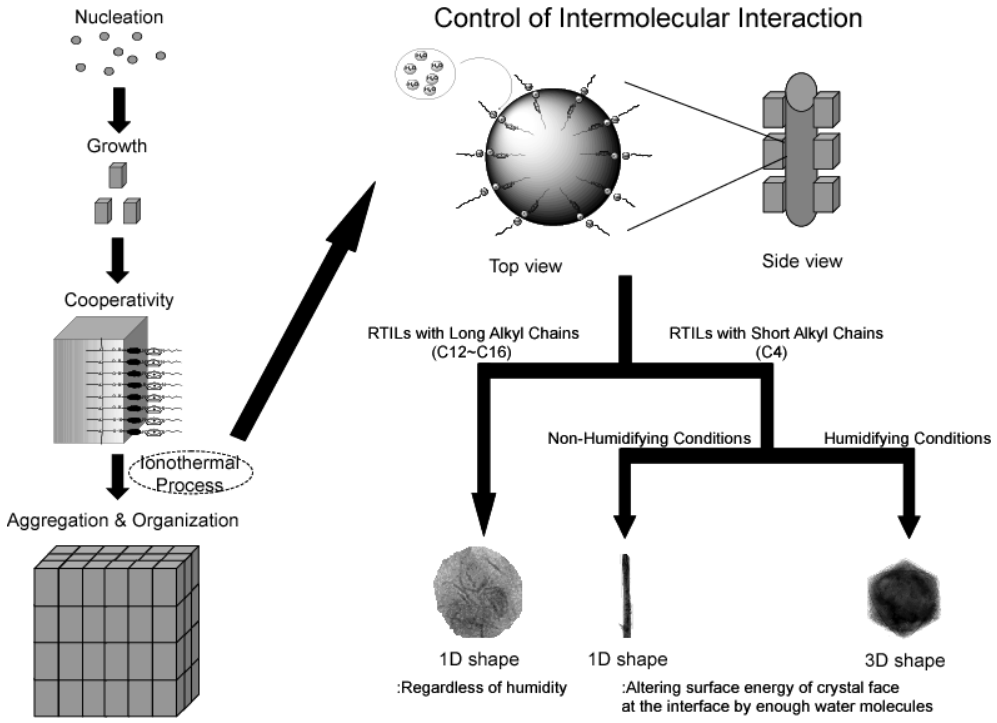

Scheme 2. The proposed formation mechanism of 1D and 3D shaped RTIL–Al hybrids via an ionothermal process depending on the anion moieties, alkyl chain length of RTILs, and humidity.

ing membrane such as Nafion, the organic–inorganic hybrid membranes mixed with heteropolyacids, and biomolecules composite materials,[23] displaying the disappearance of the semicircle at a high frequency as a result of good contact between the electrodes and the gel electrolyte.[12] The dependence between logσ and the reciprocal of the temperature was plotted using the Arrhenius equation in a range of 25–80 °C. The activation energy of the proton conduction was 20.5 kJ mol^{-1} for the Hum-C_4BF_4–Al hybrid and 19.5 kJ mol^{-1} for the Non-C_4BF_4–Al hybrid, suggesting that acid–base pairs between protonated imidazolium rings and tetrafluoroborate anions transferred protons via a Grotthus-type mechanism.[12,24] The twofold higher proton conductivities of the Hum-C_4BF_4–Al hybrid (5.8×10^{-4} to 1.1×10^{-2} S cm^{-1} at 25–80 °C) compared to those of the Non-C_4BF_4–Al hybrid (2.7×10^{-4} to 4.5×10^{-3} S cm^{-1} at 25–80 °C) were likely due to the diverse directions of the respective proton conducting pathways, as the transportation or conduction properties can be altered by the orientation of nanometer-sized channels attributed to shapes with different dimensions.[25] In addition, the irregular orientation (some of the locally dark spots in Figure 1d resulted from an irregular orientation), random de-bundling, and lower content of the structured water in the Non-C_4BF_4–Al hybrid also might decrease the proton conductivity. Taking into consideration that the proton conductivities of the C_4BF_4–Al nanohybrids were one order of magnitude higher than those of the C_4BF_4/AlOOH mixture despite a lower molar fraction of C_4BF_4, the proton conduction was facilitated by the continuous channels and the nanoconfinement effect in the system of the shape-controlled hybrids. RTILs, which were spatially confined within the pores of inorganic networks on a nanoscale, were reported to provide interesting results such as excellent catalytic activities, good proton conductivities, high heat resistances, and melting point depression, despite not yet revealing clear theoretical interpretation about the confinement effect.[11,12] In addition, N_2 adsorption/desorption isotherms represent two interpenetrating continuous networks of RTILs and aluminum hydroxides, indicating the construction of efficient proton conduction channels through interconnected pores.[26] Therefore, these nanohybrids transport cations or protons by means of ionic species of RTILs confined within the mesopores.

3. Conclusion

We demonstrate that tuning cooperative interactions between RTILs and building blocks during an ionothermal process induces various 1D and 3D nanoshapes of RTIL–Al hybrids. This synthetic process provides an effective way to develop new shapes of crystalline inorganic nanomaterials for emerging applications through an adjustment of the interplay between the RTILs and the building blocks, which is dependant on the humidifying conditions and the types of RTILs used. The shape-controlled integrated nanohybrids have better electrochemical properties than those of a conventional hybrid, exhibiting tenfold or higher proton conductivity and thermal stability as a result of continuous proton conduction channels and confinement effect.

ADVANCED FUNCTIONAL MATERIALS

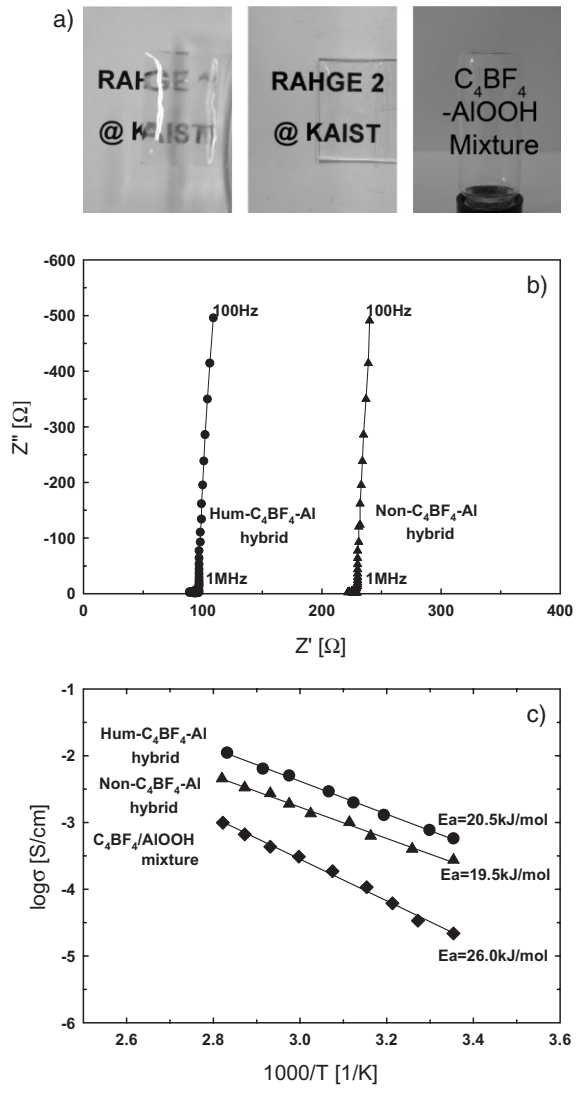

Figure 6. a) Gel films of Hum-C_4BF_4–Al (RAHGE 1) and Non-C_4BF_4–Al (RAHGE 2) hybrids spincoated on glass (3000 rpm, for 1 min) and C_4BF_4/AlOOH mixture (aluminum hydroxides (AlOOH) were prepared without C_4BF_4 under the same condition as Non-C_4BF_4–Al hybrids and mixed mechanically with C_4BF_4 at 30 wt%). b) Typical impedance responses (Cole–Cole plots) of Hum-C_4BF_4–Al and Non-C_4BF_4–Al hybrids. c) Proton conductivities of C_4BF_4–Al mixture, Hum-C_4BF_4–Al hybrid, and Non-C_4BF_4–Al hybrid at 25–80 °C.

4. Experimental

Materials: All chemicals used were analytical grade and used without further purification. 1-butyl-3-methylimidazolium tetrafluoroborate (C_4BF_4, high purity 99.9 %), 1-butyl-3-methylimidazolium bis(trifluoromethylsulfonyl)imide (C_4TFSI, high purity 99.9 %), 1-butyl-3-methylimidazolium chloride (C_4Cl, high purity 99.9 %), 1-dodecyl-3-methylimidazolium chloride (C_{12}Cl, high purity 99.9 %), and 1-hexadecyl-3-methylimidazolium chloride (C_{16}Cl, high purity 99.9 %) were supplied by C-TRI. All RTILs were stored in a vacuum oven at room temperature to avoid humidity and air contamination. Aluminum tri-*sec*-butoxide (Aldrich, 99.9 %) was used as aluminum precursor without further purification. 1-propanol and HCl were supplied by Aldrich.

Preparation of RTIL–Al Hybrids: 2.618 g of aluminum tri-*sec*-butoxide was mixed with 3 mL of 1-propanol, 0.1 mL of deionized water, and 0.995 g of C_4BF_4, respectively. 0.3 mL of 0.01 M HCl was added to the mixture dropwise. HCl was used as an acid catalyst because self-assembly via the hydrogen bonding-co-π–π stacking mechanism occurs under acidic condition as reported previously[4]. The resulting mixture was stirred at 60 °C for 120 min, followed by aging at 60 °C for 1 day. In order to complete gelation during an ionothermal synthesis, the mixture was heated to 120 °C for 2 days under ambient pressure. C_4BF_4–Aluminum hydroxide hybrid was abbreviated as Hum-C_4BF_4–Al hybrid under the humidifying condition (saturated humidity at 120 °C) and Non-C_4BF_4–Al hybrid under nonhumidifying condition (ca. 40 % humidity at 120 °C). For the purpose of verifying the templating and co-solvent functions of RTILs during an ionothermal process, the construction of nanostructured hybrids was also observed by transmission electron microscopy (TEM) and XRD, after removing volatile solvents such as water and 1-propanol by evacuation under vacuum before the ionothermal treatment. Aluminum hydroxide was isolated by extracting C_4BF_4 with acetonitrile at 60 °C. The complete removal of C_4BF_4 was confirmed by elemental analysis. In order to prove the possibility of tuning various shaped materials depending on the types of anions and the alky chain length of RTILs and the humidity, we synthesized the shaped hybrids by using C_4TFSI, C_4Cl, C_{12}Cl, and C_{16}Cl under the same experimental condition and stoichiometry as the C_4BF_4–Al hybrids. After casting thin films on glass by a spin coater (3000 rpm, for 1 min), Hum-C_4BF_4–Al and Non-C_4BF_4–Al hybrids were notated as room temperature ionic liquids–aluminum hydroxide hybrid gel electrolyte 1 and 2 (RAHGE 1 and 2), respectively. Aluminum hydroxide (AlOOH) was prepared without C_4BF_4 under the same condition as the Non-C_4BF_4–Al hybrid and mixed mechanically with C_4BF_4 of 60 wt %, in order to confirm the effect of the one-pot assembly on proton conductivity. The C_4BF_4/AlOOH mixture was a yellow high viscous gel with 60 wt % C_4BF_4 and a yellow powder with 30 wt % C_4BF_4.

Characterization: The complete removal of C_4BF_4 was confirmed by evaluating the content of carbon and nitrogen of the isolated aluminum hydroxides by means of elemental analysis. SEM images were obtained using a field emission scanning electron microscope (Philips SEM 535M) equipped with a Schottky-based field-emission gun. TEM images were collected on an E.M. 912 Ω energy-filtering transmission electron microscope (EFTEM, 120 kV) and a JEM-3010 high-resolution transmission electron microscope (HRTEM, 300 kV). X-ray diffraction (XRD) data were obtained on a Rigaku D/max IIIC (3 kW) with a θ/θ goniometer equipped with a Cu Kα radiation generator. The diffraction angle of the diffractograms was in the range of $2\theta = 10$–$80°$. FT-IR spectra were collected on a JASCO FT-IR 470 plus in attenuated total reflection mode. Each spectrum, which was recorded as the average of 12 scans with a resolution of 4 cm^{-1}, was collected from 4000 cm^{-1} to 650 cm^{-1}. ^{1}H NMR spectra were obtained by using a 400 MHz solid state NMR spectrometer (Bruker, DSX 400) with CP/MAS probe. d_6-DMSO was used as solvent. The proton conductivity of membranes was measured by the AC impedance spectroscopy over a frequency range of 10^{-1} Hz to 10^6 Hz at 10 mV. A system based on a Solatron 1255 frequency response analyzer was used to measure the proton conductivity of membranes with a two-point probe cell. The conductivity of the sample was obtained from complex impedance analysis. The real and imaginary parts of the complex impedance were plotted and the proton conductivity was obtained from the bulk resistance found in the complex impedance diagram. The proton conductivity can be calculated by using the equation $\sigma = L/RA$, where L (5 mm) and A ($0.7 \times 0.7 = 0.49$ cm^2) are the thickness of the sample and the surface area of the electrode, respectively and R is the resistance from the impedance data. In order to remove the effect of physisorbed water on the proton conductivities and evaluate ionic transport properties of only hybrids, all samples were dried under vacuum at 60 °C for 1 week before measurement. Proton conductivities of all samples were measured from 25 to 80 °C under a dry N_2 flow (anhydrous condition). Thermogravimetric analyses were carried out using a Dupont 2200 thermal analysis station. Every sample was heated from 30 to 700 °C at

a rate of 10 °C min^{-1} under a nitrogen atmosphere. N_2 sorption/desorption data was obtained using a gas sorption analyzer (NOVA 4200 Ver. 7.10). The pore size was determined using the Barrett–Joiner–Halenda (BJH) model.

Received: October 9, 2006
Revised: February 9, 2007
Published online: August 2, 2007

[1] a) C. M. Lieber, *Solid State Commun.* **1998**, *107*, 607. b) X. Peng, L. Manna, W. Yang, J. Wickham, E. Scher, A. Kadavanich, A. P. Alivisatos, *Nature* **2000**, *404*, 59. c) J. T. Hu, T. W. Odom, C. M. Lieber, *Acc. Chem. Res.* **1999**, *32*, 435. d) Y. Xia, P. Yang, Y. Sun, Y. Wu, B. Mayer, B. Gates, Y. Yin, F. Kim, H. Yan, *Adv. Mater.* **2003**, *15*, 353.

[2] a) Y. J. Zhu, W. W. Wang, R. J. Qi, X. L. Hu, *Angew. Chem. Int. Ed.* **2004**, *43*, 1410. b) Y. Jiang, Y. J. Zhu, *J. Phys. Chem. B* **2005**, *109*, 4361.

[3] a) M. A. Firestone, M. L. Dietz, S. Seifert, S. Trasobares, D. J. Miller, N. J. Zaluzec, *Small* **2005**, *1*, 754. b) Y. Liu, M. Wang, Z. Li, H. Liu, P. He, J. Li, *Langmuir* **2005**, *21*, 1618. c) B. Lee, H. Luo, C. Y. Yuan, J. S. Lin, S. Dai, *Chem. Commun.* **2004**, 240.

[4] a) H. S. Park, S. H. Yang, Y. S. Jun, W. H. Hong, J. K. Kang, *Chem. Mater.* **2007**, *19*, 535. b) Y. Zhou, J. H. Schattka, M. Antonietti, *Nano Lett.* **2004**, *4*, 477.

[5] a) X. W. Wu, H. Y. Jin, Z. Liu, T. Ohsuna, O. Terasaki, K. Sakamoto, S. N. Che, *Chem. Mater.* **2006**, *18*, 241. b) Y. W. Jun, J. W. Seo, S. J. Oh, J. W. Cheon, *Coord. Chem. Rev.* **2005**, *249*, 1766. c) S. D. Sims, D. Walsh, S. Mann, *Adv. Mater.* **1998**, *10*, 151. d) J. E. Meegan, A. Aggeli, N. Boden, R. Brydson, A. P. Brown, L. Carrick, A. R. Brough, A. Hussain, R. J. Ansell, *Adv. Funct. Mater.* **2004**, *14*, 31. e) C. Yu, B. Tian, J. Fan, G. D. Stucky, D. Zhao, *J. Am. Chem. Soc.* **2002**, *124*, 4556.

[6] a) E. R. Cooper, C. D. Andrews, P. S. Wheatley, P. B. Webb, P. Wormald, R. E. Morris, *Nature* **2004**, *430*, 1012. b) E. R. Parnham, P. S. Wheatley, R. E. Morris, *Chem. Commun.* **2006**, 380. c) E. R. Parnham, R. E. Morris, *J. Am. Chem. Soc.* **2006**, *128*, 2204.

[7] H. Cölfen, S. Mann, *Angew. Chem. Int. Ed.* **2003**, *42*, 2350.

[8] H. Cölfen, M. Antonietti, *Angew. Chem. Int. Ed.* **2005**, *44*, 5576.

[9] a) R. T. Carlin, J. Fuller, *Chem. Commun.* **1997**, 1345. b) J. Sun, L. R. Jordan, M. Forsyth, D. R. MacFarlane, *Electrochim. Acta* **2001**, *46*, 1703. c) V. Jovanovski, E. Stathatos, B. Orel, P. Lianos, *Thin Solid Films* **2006**, 634. d) C. P. Mehnert, *Chem. Eur. J.* **2005**, *11*, 50. e) A. Riisager, R. Fehrmann, M. Haumann, P, Wasserscheid, *Eur. J. Inorg. Chem.* **2006**, 695.

[10] a) A. Noda, M. A. B. H. Susan, K. Kudo, S. Mitsushima, K. Hayamizu, M. Watanabe, *J. Phys. Chem. B* **2003**, *107*, 4024. b) K. D. Kreuer, A. Fuchs, M. Ise, M. Spaeth, J. Maier, *Electrochim. Acta* **1998**, *43*, 1281.

[11] a) M. A. Néouze, J. L. Bideau, P. Gaveau, S. Bellayer, A. Vioux, *Chem. Mater.* **2006**, *18*, 3931. b) M. A. Néouze, J. L. Bideau, F. Leroux, A. Vioux, *Chem. Commun.* **2005**, 1082. c) M. Kanankubo, Y. Hiejima, K. Minami, T. Aizawa, H. Nanjo, *Chem. Commun.* **2006**, 1828. d) Y. Liu, M. Wang, J. Li, Z. Li, P. He, H. Liua, J. Li, *Chem. Commun.* **2005**, 1779. e) Z. Fei, T. J. Geldbach, D. Zhao, P. J. Dyson, *Chem. Eur. J.* **2006**, *12*, 2122. f) F. Shi, Q. Zhang, D. Li, Y. Deng, *Chem. Eur. J.* **2005**, *11*, 5279. g) F. Shi, Q. Zhang, Y. Gu, Y. Deng, *Adv. Synth. Catal.* **2005**, *347*, 225.

[12] Z. Y. Li, H. T. Liu, Y. Liu, P. He, J. H. Li, *J. Phys. Chem. B* **2004**, *108*, 17512.

[13] P. Colomban, J. P. Boilot, A. Kahn, G. Lucazeau, *Nouv. J. Chim.* **1978**, *2*, 21.

[14] H. Y. Zhu, J. D. Riches, J. C. Barry, *Chem. Mater.* **2002**, *14*, 2086.

[15] a) H. C. Lee, H. J. Kim, C. H. Rhee, K. H. Lee, J. S. Lee, S. H. Chung, *Microporous Mesoporous Mater.* **2005**, *79*, 61. b) H. Y. Zhu, X. P. Gao, D. Y. Song, S. P. Ringer, Y. X. Xi, R. L. Frost, *Microporous Mesoporous Mater.* **2005**, *85*, 226. c) H. Y. Zhu, X. P. Gao, D. Y. Song, Y. Q. Bai, S. P. Ringer, Z. Gao, Y. X. Xi, W. Martens, J. D. Riches, R. L. Frost, *J. Phys. Chem. B* **2004**, *108*, 4245. d) S. C. Kuiry, E. Megen, S. D. Patil, S. A. Deshpande, S. Seal, *J. Phys. Chem. B* **2005**, *109*, 3868.

[16] a) B. Tang, J. Ge, L. Zhuo, G. Wang, J. Niu, Z. Shi, Y. Dong, *Eur. J. Inorg. Chem.* **2005**, 4366. b) T. S. Ahmadi, Z. L. Wang, T. C. Green, A. Henglein, M. A. El-Sayed, *Science* **1996**, *272*, 1924. c) W. S. Seo, J. H. Shim, S. J. Oh, E. K. Lee, N. H. Hur, J. T. Park, *J. Am. Chem. Soc.* **2005**, *127*, 6188.

[17] M. Antonietti, D. Kuang, B. Smarsly, Y. Zhou, *Angew. Chem. Int. Ed.* **2004**, *43*, 4988.

[18] A. J. Carmichael, K. R. Seddon, *J. Phys. Org. Chem.* **2000**, *13*, 591.

[19] M. Koel, *Proc. Est. Acad. Sci., Chem.* **2000**, *49*, 145.

[20] S. C. Kuiry, E. Megen, S. D. Patil, S. A. Deshpande, S. Seal, *J. Phys. Chem. B* **2005**, *109*, 3868.

[21] a) S. C. Kuiry, E. Megen, S. D. Patil, S. A. Deshpande, S. Seal, *J. Phys. Chem. B* **2005**, *109*, 3868. b) C. P. Cho, C. A. Wu, T. P. Perng, *Adv. Funct. Mater.* **2006**, *16*, 819.

[22] a) S. H. Yu, H. Cölfen, *J. Mater. Chem.* **2004**, *14*, 2124. b) G. Wulff, *Z. Krystallogr.* **1901**, *34*, 449.

[23] M. T. Colomer, *Adv. Mater.* **2006**, *18*, 371.

[24] D. Raducha, W. Wieczorek, Z. Florjanczyk, J. R. Stevens, *J. Phys. Chem.* **1996**, *100*, 20126.

[25] C. Burda, X. Chen, R. Narayanan, M. A. El-Sayed, *Chem. Rev.* **2005**, *105*, 1025.

[26] a) M. A. Néouze, J. L. Bideau, F. Leroux, A. Vioux, *Chem. Commun.* **2005**, 1082. b) S. Dai, Y. H. Ju, H. J. Gao, J. S. Lin, S. J. Pennycook, C. E. Barnes, *Chem. Commun.* **2000**, 243.